Advances in Nano Research, *Vol. 10, No. 2 (2021) 151-163*
DOI: https://doi.org/10.12989/anr.2021.10.2.151

Geometrically nonlinear thermo-mechanical analysis of graphene-reinforced moving polymer nanoplates

Mostafa Esmaeilzadeh[1], Mohammad Esmaeil Golmakani[1], Mehran Kadkhodayan[2], Mohammadreza Amoozgar[3] and Mahdi Bodaghi*[4]

[1]*Department of Mechanical Engineering, Mashhad Branch, Islamic Azad University, Mashhad 9187144123, Iran*
[2]*Department of Mechanical Engineering, Ferdowsi University of Mashhad, Mashhad 9177948944, Iran*
[3]*School of Computing and Engineering, University of Huddersfield, HD1 3DH, United Kingdom*
[4]*Department of Engineering, School of Science and Technology, Nottingham Trent University, Nottingham NG11 8NS, United Kingdom*

(*Received May 27, 2020, Revised November 11, 2020, Accepted December 9, 2020*)

Abstract. The main target of this study is to investigate nonlinear transient responses of moving polymer nano-size plates fortified by means of Graphene Platelets (GPLs) and resting on a Winkler-Pasternak foundation under a transverse pressure force and a temperature variation. Two graphene spreading forms dispersed through the plate thickness are studied, and the Halpin-Tsai micro-mechanics model is used to obtain the effective Young's modulus. Furthermore, the rule of mixture is employed to calculate the effective mass density and Poisson's ratio. In accordance with the first order shear deformation and von Kármán theory for nonlinear systems, the kinematic equations are derived, and then nonlocal strain gradient scheme is used to reflect the effects of nonlocal and strain gradient parameters on small-size objects. Afterwards, a combined approach, kinetic dynamic relaxation method accompanied by Newmark technique, is hired for solving the time-varying equation sets, and Fortran program is developed to generate the numerical results. The accuracy of the current model is verified by comparative studies with available results in the literature. Finally, a parametric study is carried out to explore the effects of GPL's weight fractions and dispersion patterns, edge conditions, softening and hardening factors, the temperature change, the velocity of moving nanoplate and elastic foundation stiffness on the dynamic response of the structure. The result illustrates that the effects of nonlocality and strain gradient parameters are more remarkable in the higher magnitudes of the nanoplate speed.

Keywords: axially moving plates; graphene reinforced composites; thermal gradient; hybrid numerical method

1. Introduction

Due to their combined advantages of high stiffness and low self-weight, carbon-filled composites have attracted a huge interest in recent years (Medani *et al*. 2019, Bendenia *et al*. 2020, Bourada *et al*. 2020, Bousahla *et al*. 2020, Tayeb *et al*. 2020). With implementation of ABAQUS/ Explicit FEM, Pashmforoush (2020) simulated the low velocity impact of a carbon nanotube reinforced CFR polymer composite. In another study, Draoui *et al*. (2020) analyzed the static and dynamic behavior of carbon nanotube-reinforced composite sandwich plates using first-order shear deformation theory. Scholars have revealed that mechanical, electrical and thermal properties of polymer composites may be improved when small quantities of carbon nanoparticles are accrued Zhu *et al*. (2007). For example, Rafiee *et al*. (2009) showed that adding 0.1% of graphene nanoplatelets to an epoxy matrix increases its Young's modulus by 31%. Also, it is shown that graphene has greater heat conductivity capacity than copper and silver (Shen *et al*. 2017). These properties make graphene a practical candidate which can be used in different fields such as energy storage, heat spreaders, etc (Al-Mashat *et al*. 2010).

Despite the fact that there have been several experimental studies on graphene performances, it should be appreciated that graphene nanoplatelet theorical research is still in its early stages. Using finite element method, Wang *et al*. (2019a) showed the great impact of graphene nanoplatelets (GPLs) on buckling behaviours of nanocomposite shells. Wu *et al*. (2017) and Song *et al*. (2017) reported that by incorporating 0.1% of graphene nanoparticles (in a non-uniform way) into a polymer matrix, a significant improvement was achieved. The vibrational performance of functionally graded (FG) multilayer composite plates with diverse thicknesses and GPL distributions was analysed by Reddy *et al*. (2018). Hanifehlou and Mohammadimehr (2020) used different shear deformation theories to analyze buckling behaviors of GPL-reinforced sandwich beams with imperfect cores. Using Generalized Differential Quadrature Method (GDQM), Al-Furjan *et al*. (2020a) studied the nonlinear frequency and chaotic responses and also the buckling temperature and post-buckling behaviors (Al-Furjan *et al*. 2020c) of nano-composite structures. Al-Furjan *et al*. (2020d) also utilized Hamilton's principle and Von Karman nonlinear theory to investigate the nonlinear frequency and chaotic responses of the multi-scale hybrid nanocomposites reinforced disk (MHCD) embedded in a viscoelastic media

*Corresponding author, Ph.D.,
E-mail: mahdi.bodaghi@ntu.ac.uk

ISSN: 2287-237X (Print), 2287-2388 (Online)

and subject to a harmonic load. In another study, the rule of mixture and the modified Halpin-Tsai model were employed to the analysis of characteristics of the propagated wave in a sandwich solid structure with a soft core and multi-hybrid nanocomposite (MHC) face sheets (Al-Furjan *et al*. 2020b).

Nano-sized structures have attracted increasing interest by the scientific communities due to their exceptional thermal, physical, electrical, and mechanical properties (Hussain *et al*. 2019). They can be utilized in different devices such as nanoelectro-mechanical systems (NEMS), probe tips of scanning probe microscope (SPM) and tips of nano-indenter. However, the classical continuum theories of elasticity do not have an ability to accurately predict mechanical performances of micro-size structures. Therefore, novel theories have been developed to model nano-scale solids (Shishesaz *et al*. 2020, Asghar *et al*. 2020, Balubaid *et al*. 2020, Bellal *et al*. 2020). Using the theory of nonlocal elasticity along with the quasi 3D high shear deformation approach (quasi 3D HSDT), Boutaleb *et al*. (2019) studied dynamic behavior of functionally graded rectangular-shaped plates. Berghoti *et al*. (2019) performed an investigation into vibrational performance of functionally graded nanobeams using nonlocal nth-order shear deformation theory.

Strain gradient theories of elasticity are used for calculation of the size effect: Materials in micro-structures show a stiffer elastic response, e.g., during bending (Liebold and Müller 2015). In this study, the nonlocal strain gradient approach is used because this theory can entirely scrutinize the properties of the nonlocal and strain gradient parameters, respectively (Barati 2018). Liu *et al*. (2019) used a nonlocal strain gradient along with Euler-Bernoulli beam theories to scrutinize the impacts of material scale factors on the free vibration of porous sandwich small-size beams with nonlinearity features. Recently, Wang *et al*. (2019b) dealt with the nonlinear bending of FG nanocomposite beams in which graphene nanoparticle's weight coefficients changed in the axial direction.

Many engineering machines have moving continuum such as satellites, aircraft's airframes, marine apparatus and road transportation modes, etc. Owing to such applications, some studies have been conducted based upon classical elasticity theories (Esmaeilzadeh and Kadkhodayan 2018, Zhang *et al*. 2015). In the case of non-local mechanical models, Arani *et al*. (2016) conducted a study on nonlocal vibrations of an axially moving nanosheet supported by a visco-Pasternak basis exposed to a magnetic field. The nonlocal elasticity theory was used by Lim *et al*. (2015) and Li *et al*. (2017), respectively, to investigate natural frequencies of axially moving nanobeams and nanoplates. Based on the nonlocal strain gradient approach, Esmaeilzadeh and Kadkhodayan (2019b) showed nano-scale effects on dynamic behaviors of longitudinally moving GPL reinforced micro/nano sandwich plates with porosity.

Solid structures under thermomechanical loadings have been widely investigated in various research. Abualnour *et al*. (2019) proposed a novel theory, called "four variable trigonometric plate theory", to analyze the thermo-

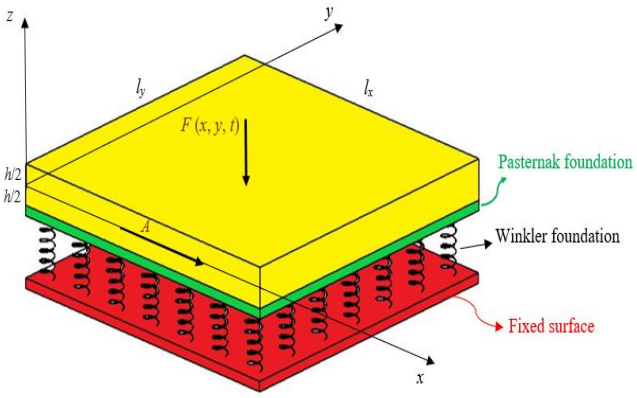

Fig. 1 A 3D schematic of a moving nanoplate mounted on an elastic foundation

mechanical bending behavior of the antisymmetric cross-ply laminates. Using finite element technique, Akbaş (2019) investigated nonlinear response of a functionally graded cantilever beam under hygro-thermal loading. Governing equations on the basis of the principle of virtual work, Boussoula *et al*. (2020) investigated thermomechanical bending of diverse outlines of FG sandwich plates. In another research, the effects of some parameters such as moisture concentration and temperature on the static behavior of advanced functionally graded (AFG) ceramic-metal plates were investigated by Tounsi *et al*. (2020). Researches are also willing to investigate the effects of the presence of elastic foundations on structures' behaviors. For example, Matouk *et al*. (2020) studied the influences of the hygro-thermal conditions on the free vibrational response of functionally graded nano-beams resting on elastic foundations. Similarly, Refrafi *et al*. (2020) performed a study to investigate the impacts of some environmental factors as well as parameters of an elastic foundation on the hygrothermal and mechanical buckling behaviors of simply supported FG sandwich plates. Mahmoudi *et al*. (2019) developed a refined quasi-three-dimensional shear deformation theory to analyze thermomechanical behavior of functionally graded sandwich plates supported by a two-parameter elastic foundation. There are also other papers in open literature (Rabhi *et al*. 2020, Chikr *et al*. 2020, Kaddari *et al*. 2020, Bellal *et al*. 2020).

In accordance with the best knowledge of the authors, there have been no papers published regarding geometrically non-linear dynamic analysis of a graphene-reinforced moving nano-size plate under thermo-mechanical loads and resting on elastic foundations. Two graphene distributions are investigated in this study and their results are compared. In this regard, it is intended to use the improved dynamic relaxation (DR) with kinetic damping method to solve governing equations. Finally, influence of some key parameters including GPL volume fractions and distribution layouts, nano-scale systems, temperature field and the nanoplate speed on the dynamic performances is numerically investigated. The results show that as the values of the nanoplate velocity increase, the significance of nonlocality and strain gradient factors on transient behaviors become more noticeable.

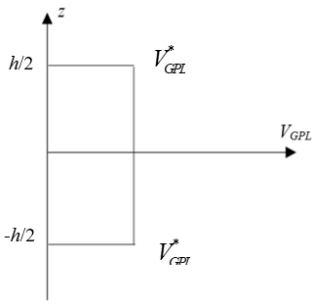

(a) Pattern A

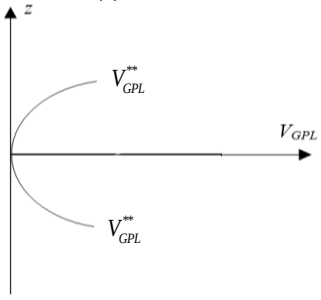

(b) Pattern B

Fig. 2 Two types of GPL distributions

2. GPL distribution patterns

Fig. 1 shows a moving supported rectangular nanoplate with graphene nanoplatelet inclusions and geometrical features of length l_x, width l_y and thickness h. Besides, (x, y, z) are axes of the Cartesian coordinate system situated on the mid-plane of the under-examined sheet. It is assumed that the plate moves along the x direction with a constant pace, A, and the graphene nanoplatelet's volume fraction, V_{GPL}, changes gradually through the thickness. In this investigation, Halpin–Tsai micromechanics model (Yang *et al*. 2018) is used to estimate effective Young's modulus E_t of the polymer nanocomposite with nano-scale fibers

$$E_t = \frac{3}{8}\left(\frac{1+\Gamma_L{}^{GPL}\chi_L{}^{GPL}V_{GPL}}{1-\chi_L{}^{GPL}V_{GPL}}\right)E_M + \frac{5}{8}\left(\frac{1+\Gamma_W{}^{GPL}\chi_W{}^{GPL}V_{GPL}}{1-\chi_W{}^{GPL}V_{GPL}}\right)E_M \tag{1}$$

in which E_M is Young's modulus of the isotropic polymer matrix. Moreover, Γ^{GPL} and χ^{GPL} symbolize the nano-particles' geometric factors, and they are described as Chen *et al*. (2017)

$$\begin{cases} \Gamma_W^{GPL} = \dfrac{2b_{GPL}}{h_{GPL}}, \qquad \Gamma_L^{GPL} = \dfrac{2a_{GPL}}{h_{GPL}} \\ \chi_L^{GPL} = \dfrac{(E_{GPL}/E_M)-1}{(E_{GPL}/E_M)+\Gamma_L^{GPL}} \\ \chi_W^{GPL} = \dfrac{(E_{GPL}/E_M)-1}{(E_{GPL}/E_M)+\Gamma_W^{GPL}} \end{cases} \tag{2}$$

where b_{GPL}, a_{GPL}, h_{GPL} and E_{GPL} denote the width, length, thickness and Young's modulus of graphene nano-fillers, respectively. Furthermore, Fig. 2 illustrates two different distribution patterns of GPLs, designated by A and B, whose volume coefficient can be measured by Chen *et al*. (2017)

$$V_{GPL} = \begin{cases} V^*_{GPL} & \text{Pattern A} \\ V^{**}_{GPL}\left[1-\cos\left(\dfrac{\pi z}{h}\right)\right] & \text{Pattern B} \end{cases}$$
$$V^{**}_{GPL} = \frac{\int_{-h/2}^{h/2} dz}{\int_{-h/2}^{h/2}\left[1-\cos\left(\frac{\pi z}{h}\right)\right]dz} V^*_{GPL} \tag{3}$$

and

$$V^*_{GPL} = \frac{\hat{\mathrm{A}}\rho_M}{\hat{\mathrm{A}}(\rho_M-\rho_{GPL})+\rho_{GPL}} \tag{4}$$

in which $\hat{\mathrm{A}}$ is the weight fraction of GPLs in the composite plate. The mass density (ρ_t), Poisson's ratio (υ_t) and thermal expansion coefficient (α_t) of the nanoplate along with graphene fibers can be obtained by the rule of mixture as (Ebrahimi and Dabbagh 2019, Yang *et al*. 2017)

$$\begin{aligned} \rho_t &= V_M\rho_M + V_{GPL}\rho_{GPL} \\ \upsilon_t &= V_M\upsilon_M + V_{GPL}\upsilon_{GPL} \\ \alpha_t &= V_M\alpha_M + V_{GPL}\alpha_{GPL} \\ V_M &+ V_{GPL} = 1 \end{aligned} \tag{5}$$

in which V_M and V_{GPL} are the volume fraction of the matrix and that of GPLs, respectively. Using the micromechanics theory (Zhang *et al*. 2016), the effective thermal conductivity of the GPLs reinforced nanocomposite can be evaluated as

$$\frac{K(z)}{K_M} = 1 + \frac{V_{GPL}}{3}\left(\frac{2}{\frac{D+1}{\left(\frac{K_W}{K_M}-1\right)}} + \frac{1}{\frac{\frac{(1-D)}{2}+1}{\left(\frac{K_Z}{K_M}-1\right)}}\right) \tag{6}$$

in which K_M is the matrix's thermal conductivity and Yang *et al*. (2017)

$$D = \frac{ln\left(\left(\xi+\sqrt{\xi^2-1}\right)\xi\right)}{\sqrt{(\xi^2-1)^3}} - \frac{1}{\xi^2-1} \tag{7}$$

$$K_x = \frac{K_{GPL}}{\frac{2R_kK_{GPL}}{a_{GPL}}+1} \quad K_y = \frac{K_{GPL}}{\frac{2R_kK_{GPL}}{h_{GPL}}+1} \tag{8}$$

where R_k is an average interfacial thermal resistance between the GPLs and matrix; also, K_{GPL} signifies the inherent thermal conductivity of GPLs and $\xi = \frac{\Gamma_L^{GPL}}{2}$ (Yang *et al*. 2017).

Regarding the thermal loading problem, it is presumed that the temperature field only changes along the depth and is established by Golmakani and Zeighami (2017)

$$-\frac{d}{dz}\left(K(z)\frac{dT(z)}{dz}\right) = 0 \tag{9}$$

After solving this differential Eq. (9) and using the thermal boundary conditions for bottom and top surfaces as below (Golmakani and Zeighami 2017)

$$T\left(x,y,-\frac{h}{2}\right)=T_1,\qquad T(x,y,+\frac{h}{2})=T_2 \tag{10}$$

and based on Eqs. (9) and (10), the temperature function ($T(z)$) can be obtained as

$$T(z)=T_1+(T_2-T_1)\frac{\int_{-h/2}^{z}\frac{dz}{K(z)}}{\int_{-h/2}^{h/2}\frac{dz}{K(z)}} \tag{11}$$

It is essential to mention that $T(z)$ is evaluated from the room temperature (T_0 = 280K).

3. Fundamental equations

The displacement fields with the usual assumptions of the first order shear deformation theory (FSDT) are written as

$$\begin{matrix}U(x,y,z,t)=u_1(x,y,t)+z\phi_x(x,y,t)\\ V(x,y,z,t)=u_2(x,y,t)+z\phi_y(x,y,t)\\ W(x,y,z,t)=u_3(x,y,t)\end{matrix} \tag{12}$$

in which u_1, u_2 and u_3 are the displacement components in the mid-plane of the polymer nanoplate reinforced by GPLs along x, y and z axes, respectively. Furthermore, ϕ_x and ϕ_y, respectively, denote rotational dislocations about the y- and x-axis. The components of strain field with the consideration of von Kármán nonlinear relations can be expressed as

$$\begin{Bmatrix}\varepsilon_{xx}\\ \varepsilon_{yy}\\ \varepsilon_{xy}\\ \varepsilon_{yz}\\ \varepsilon_{xz}\end{Bmatrix}=\begin{Bmatrix}u_{1,x}+\frac{u_{3,x}^2}{2}+z\phi_{x,x}\\ u_{2,y}+\frac{u_{3,y}^2}{2}+z\phi_{y,y}\\ u_{1,y}+u_{2,x}+u_{3,x}u_{3,y}+z\left(\phi_{x,y}+\phi_{y,x}\right)\\ \phi_y+u_{3,y}\\ \phi_x+u_{3,x}\end{Bmatrix} \tag{13}$$

It should be noted that the subscript (,) is the derivative operator with respect to the relevant variable.

$$(1-\beta^2\nabla^2)\sigma_{ij}=C_{ijkl}(1-l^2\nabla^2)\varepsilon_{kl} \tag{14}$$

where β illustrate the influence of non-invariant stress field, l captures the strain gradient effects, and C_{ijkl} shows the elasticity tensor. ∇^2 is the Laplace operator and is equal to $\frac{\partial^2}{\partial x^2}+\frac{\partial^2}{\partial y^2}$. Thus, the nonlocal strain gradient relations of a GPL-reinforced nanoplate turns

$$(1-\beta^2\nabla^2)\begin{Bmatrix}\sigma_{xx}\\ \sigma_{yy}\\ \sigma_{xy}\\ \sigma_{yz}\\ \sigma_{xz}\end{Bmatrix}=(1-l^2\nabla^2)\times \tag{15}$$

$$\begin{bmatrix}Q_{11}&Q_{12}&0&0&0\\ Q_{21}&Q_{22}&0&0&0\\ 0&0&Q_{66}&0&0\\ 0&0&0&C_{44}&0\\ 0&0&0&0&C_{55}\end{bmatrix}\left(\begin{Bmatrix}\varepsilon_{xx}\\ \varepsilon_{yy}\\ \varepsilon_{xy}\\ \varepsilon_{yz}\\ \varepsilon_{xz}\end{Bmatrix}-\begin{Bmatrix}\alpha_tT(z)\\ \alpha_tT(z)\\ 0\\ 0\\ 0\end{Bmatrix}\right)$$

in which

$$\begin{cases}Q_{11}=Q_{22}=\dfrac{E(z)}{1-\upsilon(z)^2}\\ Q_{12}=Q_{21}=\dfrac{\upsilon(z)E(z)}{1-\upsilon(z)^2}\\ C_{44}=C_{55}=Q_{66}=G(z)=\dfrac{E(z)}{2(1+\upsilon(z))}\end{cases} \tag{16}$$

After applying the nonlocal parameter on the stress resultants and moments, they can be expressed in the nano-scale system as

$$\begin{matrix}(1-\beta^2\nabla^2)(N_i,M_i)=\left(\widetilde{N}_i,\widetilde{M}_i\right)\\ =(1-\beta^2\nabla^2)\left(\int_{-\frac{h}{2}}^{\frac{h}{2}}(1,z)\sigma_i dz\right)\\ (i=xx,yy,xy)\end{matrix} \tag{17}$$

$$\begin{matrix}(1-\beta^2\nabla^2)Q_i=\tilde{Q}_i\\ =K^2(1-\beta^2\nabla^2)\left(\int_{-h/2}^{h/2}\sigma_{iz}dz\right),\quad (i=x,y)\end{matrix} \tag{18}$$

In Eq. (18), the transverse shear correction constant, K^2, is set 0.833. With the aid of Eqs. (15)-(18), the stress resultants and moments can be expressed as

$$\begin{bmatrix}\widetilde{N}_{xx}\\ \widetilde{N}_{yy}\\ \widetilde{N}_{xy}\end{bmatrix}=(1-l^2\nabla^2)\times$$
$$\left(\begin{pmatrix}X_{11}&X_{12}&0\\ X_{12}&X_{22}&0\\ 0&0&X_{66}\end{pmatrix}\begin{bmatrix}u_{1,x}+\frac{u_{3,x}^2}{2}\\ u_{2,x}+\frac{u_{3,y}^2}{2}\\ u_{1,y}+u_{2,x}+u_{3,x}u_{3,y}\end{bmatrix}+\right.$$
$$\left.\begin{pmatrix}Y_{11}&Y_{12}&0\\ Y_{12}&Y_{22}&0\\ 0&0&Y_{66}\end{pmatrix}\begin{bmatrix}\phi_{x,x}\\ \phi_{y,y}\\ \phi_{x,y}+\phi_{y,x}\end{bmatrix}-\begin{bmatrix}N_x^{TH}\\ N_y^{TH}\\ 0\end{bmatrix}\right)$$
$$\begin{bmatrix}\widetilde{M}_{xx}\\ \widetilde{M}_{yy}\\ \widetilde{M}_{xy}\end{bmatrix}=(1-l^2\nabla^2)\times \tag{19}$$
$$\left(\begin{pmatrix}Y_{11}&Y_{12}&0\\ Y_{12}&Y_{22}&0\\ 0&0&Y_{66}\end{pmatrix}\begin{bmatrix}u_{1,x}+\frac{u_{3,x}^2}{2}\\ u_{2,x}+\frac{u_{3,y}^2}{2}\\ u_{1,y}+u_{2,x}+u_{3,x}u_{3,y}\end{bmatrix}+\right.$$
$$\left.\begin{pmatrix}Z_{11}&Z_{12}&0\\ Z_{12}&Z_{22}&0\\ 0&0&Z_{66}\end{pmatrix}\begin{bmatrix}\phi_{x,x}\\ \phi_{y,y}\\ \phi_{x,y}+\phi_{y,x}\end{bmatrix}-\begin{bmatrix}M_x^{TH}\\ M_y^{TH}\\ 0\end{bmatrix}\right)$$

$$\begin{bmatrix}\tilde{Q}_{yz}\\ \tilde{Q}_{xz}\end{bmatrix}=(1-l^2\nabla^2)\begin{bmatrix}G_{44} & 0\\ 0 & G_{55}\end{bmatrix}\begin{bmatrix}\phi_y+u_{3,y}\\ \phi_x+u_{3,x}\end{bmatrix} \tag{20}$$

where X_{ij}, Y_{ij}, Z_{ij} (i, j = 1, 2, 6) and G_{44} and G_{55} can be written as Li *et al*. (2018)

$$\begin{aligned}&\{X_{ij},Y_{ij},Z_{ij}\}=\left(\int_{-h/2}^{h/2}Q_{ij}(1,z,z^2)dz\right)\\ &G_{44}=K^2\times\left(\int_{-h/2}^{h/2}C_{44}dz\right),\ \ G_{55}=K^2\times\left(\int_{-h/2}^{h/2}C_{55}dz\right)\end{aligned} \tag{21}$$

Also, $\{N^{TH}\}$ and $\{M^{TH}\}$ signify the thermal force and thermal moment resultants, respectively, defined as

$$\begin{Bmatrix}N_x^{TH}\\ N_y^{TH}\end{Bmatrix}=\int_{-h/2}^{h/2}\begin{bmatrix}Q_{11} & Q_{12}\\ Q_{12} & Q_{22}\end{bmatrix}\alpha_t T(z)dz \tag{22}$$

$$\begin{Bmatrix}M_x^{TH}\\ M_y^{TH}\end{Bmatrix}=\int_{-h/2}^{h/2}\begin{bmatrix}Q_{11} & Q_{12}\\ Q_{12} & Q_{22}\end{bmatrix}\alpha_t T(z)zdz \tag{23}$$

The Hamilton's principal is implemented to derive dynamic equations, which states that

$$\int_0^T(\delta R+\delta P-\delta S)=0 \tag{24}$$

where R is total potential energy of a system, and also P and S are applied work and kinetic energy of the system, respectively. Also, the symbol δ shows the variation operator. The virtual potential energy can be expressed in terms of stress and strain as

$$\delta R=\iiint_V\sigma_{ij}\,\varepsilon_{ij}dV \tag{25}$$

By consideration of the velocity vector of the longitudinally moving plate, A, the kinetic energy of the plate can be written as

$$\begin{aligned}S=\frac{1}{2}\iiint_V\rho(z)\Big(&\Big(A+\frac{\partial U}{\partial t}+A\frac{\partial U}{\partial x}\Big)^2+\Big(\frac{\partial V}{\partial t}+A\frac{\partial V}{\partial x}\Big)^2\\ &+\Big(\frac{\partial W}{\partial t}+A\frac{\partial W}{\partial x}\Big)^2\Big)dzdydx\end{aligned} \tag{26}$$

with the application of variation operator, δ, on Eq. (26), this can be rewritten as

$$\begin{aligned}\delta S=\iiint_V\rho(z)\Bigg(&\Big(A+\frac{\partial U}{\partial t}+A\frac{\partial U}{\partial x}\Big)\Big(\delta A+\delta\frac{\partial U}{\partial t}\\ &+A\delta\frac{\partial U}{\partial x}\Big)+\Big(\frac{\partial V}{\partial t}+A\frac{\partial V}{\partial x}\Big)\Big(\delta\frac{\partial V}{\partial t}+A\delta\frac{\partial V}{\partial x}\Big)\\ &+\Big(\frac{\partial W}{\partial t}+A\frac{\partial W}{\partial x}\Big)\Big(\delta\frac{\partial W}{\partial t}+A\delta\frac{\partial W}{\partial x}\Big)\Bigg)dzdydx\end{aligned} \tag{27}$$

Finally, the kinematic equation of nanoplates subjected to distributed dynamic pressure loads ($F(x, y, t)$) can be formulated as

$$\begin{aligned}&\widetilde{N}_{xx,x}+\widetilde{N}_{xy,y}=(1-\beta^2\nabla^2)\left(I_0\frac{D^2u}{Dt^2}+I_1\frac{D^2\psi_x}{Dt^2}\right)\\ &\widetilde{N}_{xy,x}+\widetilde{N}_{yy,y}=(1-\beta^2\nabla^2)\left(I_0\frac{D^2v}{Dt^2}+I_1\frac{D^2\psi_y}{Dt^2}\right)\\ &\tilde{Q}_{x,x}+\tilde{Q}_{y,y}+(1-\beta^2\nabla^2)N(w)-F(x,y,t)\\ &-(1-\beta^2\nabla^2)K_w w+(1-\beta^2\nabla^2)K_s\left(\frac{\partial^2w}{\partial x^2}+\frac{\partial^2w}{\partial y^2}\right)\\ &=(1-\beta^2\nabla^2)I_0\frac{D^2w}{Dt^2}\\ &\widetilde{M}_{xx,x}+\widetilde{M}_{xy,y}-\tilde{Q}_x=(1-\beta^2\nabla^2)\left(I_1\frac{D^2u}{Dt^2}+I_2\frac{D^2\psi_x}{Dt^2}\right)\\ &\widetilde{M}_{xy,x}+\widetilde{M}_{yy,y}-\tilde{Q}_y=(1-\beta^2\nabla^2)\left(I_1\frac{D^2v}{Dt^2}+I_2\frac{D^2\psi_y}{Dt^2}\right)\\ &N(w)=N_{xx}w_{,xx}+2N_{xy}w_{,xy}+N_{yy}w_{,yy}\end{aligned} \tag{28}$$

where K_w is the Winkler foundation modulus and K_s is the Pasternak shear foundation, and

$$I_m=\int_{-\frac{h}{2}}^{\frac{h}{2}}\rho(z)z^m dz\,,\qquad m=0,1,2 \tag{29}$$

$$\frac{D^2}{Dt^2}=\frac{\partial^2}{\partial t^2}+2A\frac{\partial^2}{\partial x\partial t}+A^2\frac{\partial^2}{\partial x^2} \tag{30}$$

In order to complete the formulation, a set of edge constrains should be introduced. Herein, fully clamped (CCCC) and fully simply supported (SSSS) edge constrains are considered as

a) Fully clamped boundary conditions (CCCC)

$$\begin{cases}x=0, & l_x\to u_1=u_2=u_3=\phi_x=\phi_y=0\\ y=0, & l_y\to u_1=u_2=u_3=\phi_x=\phi_y=0\end{cases} \tag{31}$$

b) Fully simply supported boundary conditions (SSSS)

$$\begin{cases}x=0, & l_x\to u_1=u_2=u_3=\phi_y=M_{xx}=0\\ y=0, & l_y\to u_1=u_2=u_3=\phi_x=M_{yy}=0\end{cases} \tag{32}$$

4. Numerical methods

In this study, the kinetic dynamic relaxation (K-DR) method is modified by Newmark technique to solve geometrically non-linear Eq. (28) in both time and space domains. Firstly, the kinetic equations are turned into equivalent static forms by means of Newmark method, and then these transformed equations are solved by K-DR method and finite difference discretization technique.

4.1 Newmark integration method

In the Newmark method, the velocity and acceleration of the system at the next time step (j + 1) can be derived as

$$\dot{x}_{j+1}=\begin{pmatrix}\frac{\alpha}{\kappa\Delta t_j}(x_{j+1}-x_j)-\left(\frac{\alpha}{\kappa}-1\right)\dot{x}_j-\\ \left(\frac{\alpha}{2\kappa}-1\right)\Delta t_j\ddot{x}_j\end{pmatrix} \tag{33}$$

$$\ddot{x}_{j+1} = \left(\frac{1}{\kappa(\Delta t_j)^2}(x_{j+1} - x_j) - \frac{1}{\kappa \Delta t_j}\dot{x}_j - \left(\frac{1}{2\kappa} - 1\right)\ddot{x}_j \right) \tag{34}$$

where κ = 0.25 and α = 0.5 are Newmark constants. Also, x is the vector of unknown variable (u_1, u_2, u_3, ϕ_x, ϕ_y) and Δt is the difference between the current real time and the previous one. By substituting Eqs. (33)-(34) into Eq. (28), it becomes

$$[\bar{K}_{j+1}]x_{j+1} = \{\bar{P}_{j+1}\} \tag{35}$$

where $[\bar{K}_{j+1}]$ is the corresponding stiffness matrix and $\{\bar{P}_{j+1}\}$ signifies corresponding load vector, defined as (Esmaeilzadeh and Kadkhodayan 2019a)

$$[\bar{K}_{j+1}] = \frac{1}{\kappa(\Delta t_j)^2}[I_{j+1}] + [K_{j+1}] \tag{36}$$

$$\{\bar{P}_{j+1}\} = \{P_{j+1}\} + \left\{ [I_{j+1}] \left[\frac{1}{\kappa(\Delta t_j)^2} x_j + \frac{1}{\kappa \Delta t_j}\dot{x}_j + \left(\frac{1}{2\kappa} - 1\right)\ddot{x}_j \right] \right\} \tag{37}$$

In which $[I_{j+1}]$and $[K_{j+1}]$ represent the inertia and the stiffness matrices, respectively. Also, $\{P_{j+1}\}$ is the external work vector.

4.2 Kinetic dynamic relaxation technique

In this approach, to solve the nonlinear Eq. (35), they are transformed into artificial dynamic space by adding fictitious mass matrix as Esmaeilzadeh and Kadkhodayan (2019a)

$$[M]^n_{DR}\{a\}^n + [\bar{K}_{j+1}]^n x^n_{j+1} = \{\bar{P}^n_{j+1}\} \tag{38}$$

where $\{a\}^n$ and $[M]^n_{DR}$ denote, separately, the made-up acceleration vector in n^{th} iteration of the K-DR [55] and diagonal artificial mass matrix. It should be noted that numerical convergence of K-DR method can be guaranteed when the artificial mass is introduced based on the Gershgörin theorem (Alamatian 2012).

$$m^{DOF}_{ii} \geq 0.5(\tau^n)^2 \sum_{p=1}^{DOF} |k_{ip}|, \quad k_{ip} = \frac{\partial\{[\bar{K}]^n_{j+1}x^n_{j+1}\}}{\partial x} \tag{39}$$

in which m_{ii} and DOF are, respectively, fictitious mass matrix elements and the number of degrees of structures. The nodal velocity and displacement vectors at the next fictitious time step can be expressed by

$$\{v\}^{n+1/2} = v^{n-1/2} + \frac{\tau^n}{[M]_{DR}}\left(\{\bar{P}_{j+1}\} - [\bar{K}_{j+1}]x_{j+1}\right) \tag{40}$$

$$\{x\}^{n+1} = \{x\}^n + \tau^n\{v\}^{n+\frac{1}{2}} \tag{41}$$

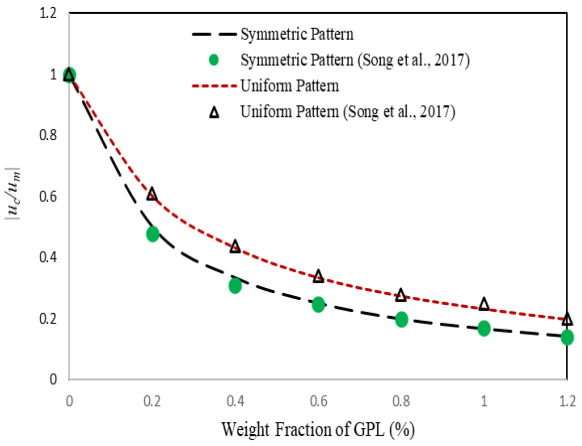

Fig. 3 Effects of GPL weight fractions on u_c/u_m of SSSS GPL/epoxy nanocomposite plates

Also, Eq. (42) is used in order to obtain the kinetic energy of the system.

$$KE^{n+1} = \frac{1}{2}\sum_{i=1}^{DOF} m^n_{ii}\,(v_i^{n+\frac{1}{2}})^2 \tag{42}$$

The kinetic energy of the system is traced through the time domain and when a maximum value is detected the current velocities are set to zero (Alic and Persson 2016). Researchers have shown that the displacement in the step of n-1/2 should be used as a starting point for the new analysis. For this purpose, the forward finite difference is used.

$$\{x\}^{n-\frac{1}{2}} = \{x\}^n - \left(\frac{3}{2}\tau^n\right)\{v\}^{n+\frac{1}{2}} + \frac{(\tau^n)^2}{2[M]^n_{DR}}\{\bar{P}^n_{j+1} - [\bar{K}_{j+1}]^n x^n_{j+1}\} \tag{43}$$

The velocity of the next step can be obtained by

$$\{v\}^{n+\frac{1}{2}} = \frac{\tau^n}{2[M_{DR}]^n}\{\bar{P}^n_{j+1} - [\bar{K}_{j+1}]^n x^n_{j+1}\} \tag{44}$$

The K-DR process keeps its running until the steady state situation happens (i.e., $|KE^{n+1}| \leq 10^{-12}$ and $\left|\{\bar{P}^n_{j+1} - [\bar{K}_{j+1}]^n x^n_{j+1}\}\right| \leq 10^{-9}$). These steps are iterated for each time increment of Newmark method.

5. Numerical results

5.1 Comparison study

Case study 1: For confirming the correctness of the extant formulation and numerical system, a simply supported plate reinforced with graphene platelets and subjected to a distributed pressure force is considered. The external forced is uniformly distributed over the upper surface of the plate, and decays linearly as the time passes. Here, the maximum magnitude of load is 500 kPa and

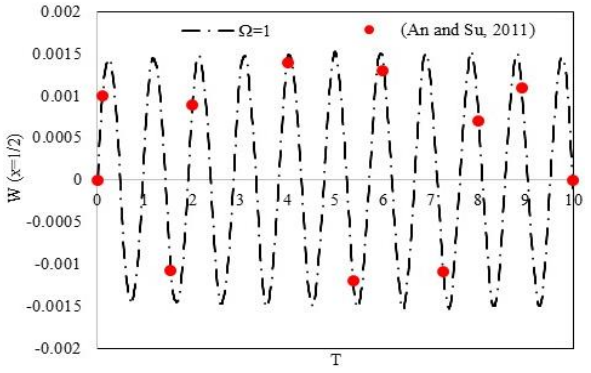

Fig. 4 Dimensionless vertical displacement at the center of a CCCC axially moving beam, $\varsigma = 0.1$

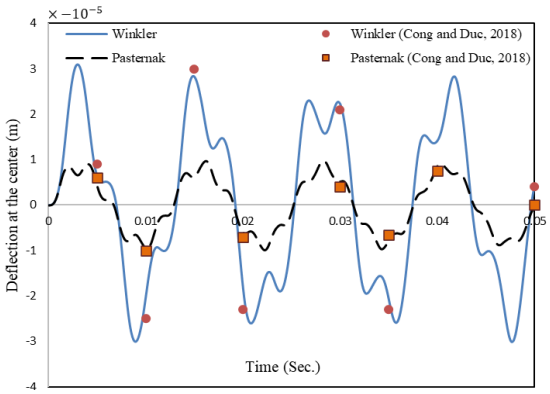

Fig. 5 Effects of elastic foundations on central dynamic deflection of a SSSS nanocomposite plate

exposed to the plate for a time-course of 0.01 S. For this example, Song *et al*. (2019) used two different types of GPL distributions, namely symmetric pattern and monotonous pattern. The dimensions and geometrical parameters of the sheet and GPLs are assumed as

$$l_x = l_y = 45 \times 10^{-2}\text{m}, \quad h = 0.45 \times 10^{-2}\ \text{m}$$
$$E_M = 3.0 \times 10^9\ \text{Pa}, \quad \rho_M = 1200\,\frac{\text{kg}}{\text{m}^3}$$
$$\upsilon_M = 0.34, \quad a_{GPL} = 2.5\ \mu\text{m}, \quad b_{GPL} = 1.5\ \mu\text{m}$$
$$h_{GPL} = 1.5\ \text{nm}, \quad E_{GPL} = 1.01 \times 10^{12}\text{Pa}$$
$$\rho_{GPL} = \frac{1060\text{kg}}{\text{m}^3}, \quad \upsilon_{GPL} = 0.18$$

The results are compared in Fig. 3 where u_c denotes the maximum time-dependent displacement of the sheet with graphene nanoplatelets and u_m is the supreme transient central deflection of the GPL-free plate. As it can be observed from Fig. 3, the obtained results are in a good correlation with those from the reference solution.

Case study 2: The comparison of non-dimensional transverse displacement at the center of a fully clamped moving beam with a constant dimensionless velocity, $\Omega = 1$ and following parameters is plotted in Fig. 4.

$$\begin{cases} W_{,tt} + 2\Omega W_{,xt} - (1-\Omega^2)W_{,xx} + \varsigma W_{,xxxx} = 0 \\ W = \dfrac{u_3}{l_x}, \quad \Omega = A\sqrt{\dfrac{\rho}{P_0}}, \quad T = t\sqrt{\dfrac{P_0}{\rho l_x^2}}, \quad \varsigma = \dfrac{EI}{P_0 l_x^2} \end{cases} \quad (45)$$

in which u_3, W, A, Ω, P_0, EI, ρ and l_x signify the transverse central displacement, non-dimensional central deflection, speed, non-dimensional speed, axial tension, bending stiffness, mass density of the structure and the length size, respectively. Furthermore, t and T are, respectively, the corresponding symbols of time and non-dimensional time. An and Su (2011) used the generalized integral transform technique to gain a hybrid analytical-numerical result for transient response of clamped axially moving beams. As seen in Fig. 4, it is evident that the obtained results and those reported in An and Su (2011) are quite close verifying the accuracy of the present solution.

Case study 3: In this section, the influence of Winkler and Pasternak types of foundation on the dynamic bending of a GPL-reinforced nanocomposite solid under a uniform harmonic force, $F(x,y,t) = 2000\sin(500t)$, with K_w = 0.1 GPa/m and K_s = 0.01 GPa.m is investigated and compared with results from Cong and Duc (2018). The following parameters are utilized.

$$l_x = l_y = 0.9\ \text{m}, \quad h = 0.045\ \text{m}$$
$$E_M = 3\ \text{GPa}, \quad \rho_M = 1200\,\frac{\text{kg}}{\text{m}^3}$$
$$\upsilon_M = 0.34, \quad a_{GPL} = 2.5\ \mu\text{m}$$
$$b_{GPL} = 1.5\ \mu\text{m}, \quad h_{GPL} = 15\ \text{nm}$$
$$E_{GPL} = 101\ \text{GPa}, \quad \rho_{GPL} = 1062.5\ \frac{\text{kg}}{\text{m}^3}$$
$$\upsilon_{GPL} = 0.186, \quad \hat{A} = 0.3\%$$

The results are presented in Fig. 5. It is observed that the value of dynamic deflection due to a Pasternak foundation is much lower than that of Winkler ones, and DR-Newmark technique is an effective method for predicting dynamic characteristics of nanocomposite plates with elastic foundations.

Case study 4: In the final example, the accuracy of the current model for micro-size structures is confirmed by comparing the results obtained for the transient responses of a fully clamped moving GPL-reinforced porous sandwich nanoplate with those given in Esmaeilzadeh and Kadkhodayan (2019b). In this case, a square plate with uniform GPL and symmetric porous distribution under a dynamic pressure force of 10 MPa (porosity fraction: 0.2 and $\hat{A}$ = 1%) and following mechanical properties is examined.

$$l_x = l_y = 200\ \text{nm}$$
$$h = 14\ \text{nm}\ (h_M = 10\ \text{nm}, h_f = 2\ \text{nm})$$
$$a_{GPL} = 2.5\ \text{nm}, \quad b_{GPL} = 1.5\ \text{nm}$$
$$h_{GPL} = 1.5 \times 10^{-3}\ \text{nm}$$
$$E_M = 116\ \text{GPa}, \quad \rho_M = 1200\ \text{kgm}^{-3}$$
$$\upsilon_m = 0.34, \quad E_f = 116\ \text{GPa}$$
$$\rho_f = 1200\ \text{kgm}^{-3}, \quad \upsilon_f = 0.34$$
$$E_{GPL} = 1.01\ \text{TPa}, \quad \rho_{GPL} = 1060\ \text{kgm}^{-3}$$
$$\upsilon_{GPL} = 0.186$$

Subscripts M, f and GPL denote, respectively, matrix,

Table 1 Comparison of the dimensionless central deflection of nanoplates with CCCC edge conditions, $\Omega = 4.0$

Boundary conditions	(*Be*, *G*)	Dimensionless central deflection	
		(u_3/h) × 10 current study	(u_3/h) × 10 Esmaeilzadeh and Kadkhodayan (2019b)
CCCC	(0, 0)	−2.91	−2.91
CCCC	(0, 0.1)	−2.79	−2.79

Table 2 Effects of elastic foundations and GPL distributions on the maximum value of non-dimensional deflection of nanoplate (CCCC)

K_s (*GPa.m*)	K_w (*GPa/m*)	W_{max}	
		GPL distribution (A)	GPL distribution (B)
0	0.0	−4.49	−0.94
	0.1	−2.28	−0.89
0.01	0.0	−1.80	−0.83
	0.1	−1.31	−0.73

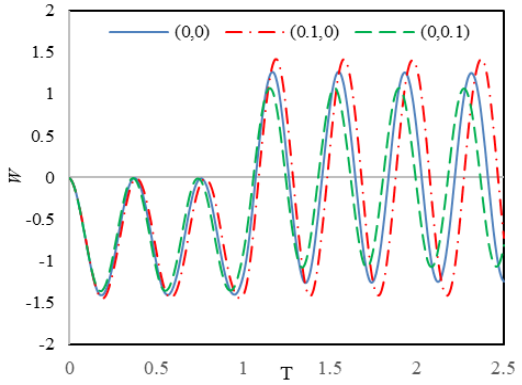

(a) Central deflection

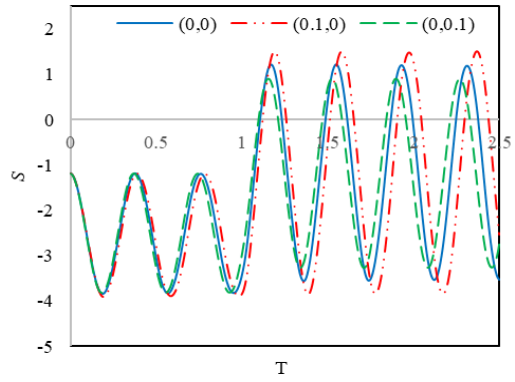

(b) Central axial moment resultant

Fig. 6 Effects of the uniform GPL distribution on the dynamic behavior of the fully clamped nanoplate for different nano-scale factors (*Be*, *G*)

face surface and graphene nanoplatelets. From Table 1, it can be seen that the present results are in excellent agreement with those reported in Esmaeilzadeh and Kadkhodayan (2019b) that shows the accuracy of the methodology and solution.

5.2 Parametric study

In this section, the effects of the elastic foundation, GPL distributions, temperature change and nano-scale parameters on dimensionless dynamic central deflection and stress field of moving micro-size plates are investigated. To do this, a square-shaped GPL-reinforced nanoplate with the following geometrical and mechanical properties is considered.

$$
\begin{aligned}
&l_x = l_y = 200\ \text{nm}, && h = 20\ \text{nm}\\
&E_M = 2.85\ \text{GPa}, && \rho_M = 1200\,\frac{\text{kg}}{\text{m}^3}\\
&\alpha_M = \frac{8.2\times10^{-5}}{K}, && K_M = 0.2\,\frac{\text{W}}{\text{mK}}\\
&\upsilon_M = 0.34,\\
&a_{GPL} = b_{GPL} = 3\ \text{nm}, && h_{GPL} = 15\times10^{-4}\text{nm}\\
&E_{GPL} = 1.01\ \text{TPa}, && \rho_{GPL} = 1060\,\frac{\text{kg}}{\text{m}^3}\\
&\alpha_{GPL} = \frac{2.35\times10^{-5}}{K}, && K_{GPL} = 2000\,\frac{\text{W}}{\text{mK}}\\
&\upsilon_{GPL} = 0.18, && R_k = 10^{-8}\,\frac{\text{m}^2\text{K}}{\text{W}}
\end{aligned}
$$

The plate is subjected to a uniform pressure force expressed by

$$
F(x,y,t) = \begin{cases} 10000000\ Pa, & t \le 0.1s \\ 0, & t > 0.1s \end{cases} \tag{46}
$$

To obtain appropriate results, the non-dimensional parameters are defined as follows

$$
\begin{aligned}
&W = \frac{u_3\left(\frac{a}{2},\frac{b}{2}\right)}{h}\times 10\\
&S = \frac{M_{xx}\left(\frac{a}{2},\frac{b}{2}\right)}{E_M h^2}\times 100\\
&\Omega = 100\times A\sqrt{\frac{\rho_M}{E_M}}, \qquad T = \frac{t}{0.1}\\
&Be = \frac{\beta^2}{l_x}, \qquad G = \frac{l^2}{l_x}
\end{aligned} \tag{47}
$$

Unless stated otherwise, the temperature is held at T_1 = 280K at the bottom surface of the plate and T_2 = 340K at the top surface. Also, Ω, $\hat{A}$, K_s and K_w are 6.49, 5%, 0.01 GPa.m and 0.1 GPa/m, respectively.

Influence of the foundation stiffness on dimensionless central deflection for two GPL distributions with weight fraction of 5% and (*Be*, *G*) = (0, 0.2) is analyzed and the results are provided in Table 2. As depicted in Table 2, the elastic foundation can result in a remarkable decrease in the dynamic dislocation in all cases. The plates with uniform GPL distribution pattern (A) undergo the largest transient deflection of −4.49 once K_w = 0 and K_s = 0 are set. In contrast, the ones with symmetric GPL distribution (B) possess the least value of transient dimensionless deflection, which is equal to −0.943. When the plates are located an elastic foundation with K_s = 0.01 GPa.m and K_w = 0.1

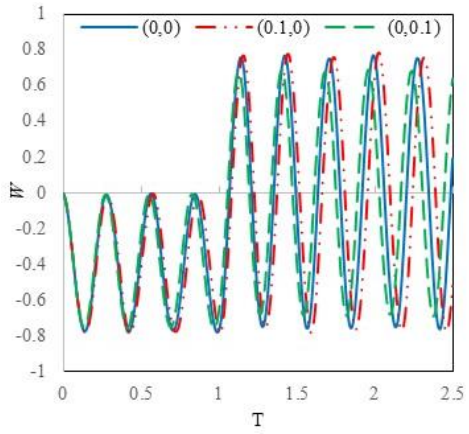

(a) Central deflection

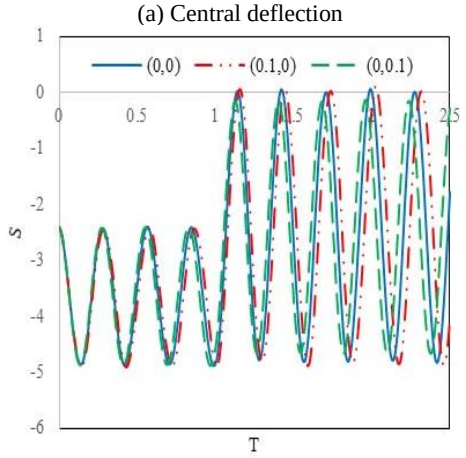

(b) Central axial moment resultant

Fig. 7 Effects of the symmetric GPL distribution on the dynamic behavior of the fully clamped nanoplate for different nano-scale factors (*Be*, *G*)

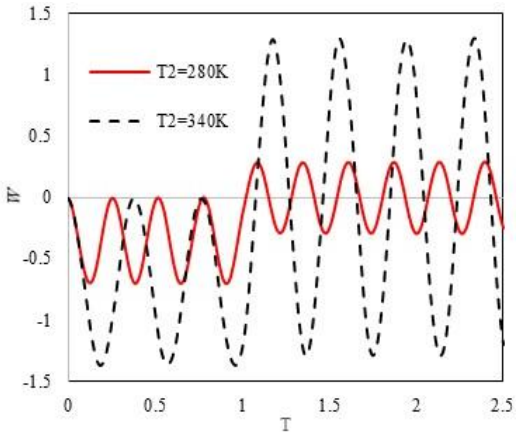

(a) Uniform GPL distribution

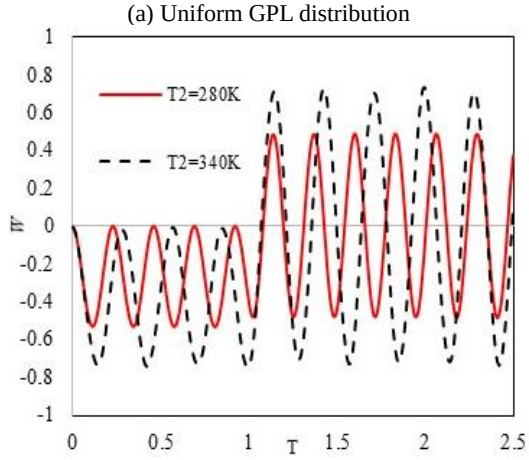

(b) Symmetric GPL distribution

Fig. 8 Effects of temperature variations on the non-dimensional central deflection of the CCCC nanoplate

GPa/m the deflections fall noticeably to −1.31 and −0.727, respectively.

Figs. 6-7 demonstrate how much the nonlocal (*Be*) and strain gradient (*G*) factors affect the dynamic deflection and axial moment resultant of a micro-size CCCC plate with a uniform GPL distribution and a symmetric distribution, respectively. It is evident that with a rise in the quantity of nonlocal factor (*Be*), a larger dynamic deflection can be seen since increasing the nonlocal parameter decreases the bending rigidity of the nanoplate. Conversely, a growth in the magnitude of strain gradient coefficient (*G*) can improve the strength of the nanosolid; hence, it leads to the decline of the amplitude of dimensionless transient vertical displacement. It is also shown that the effects of nonlocal (*Be*) and strain gradient (*G*) parameters on the nanoplate are independent of GPL distributions.

The non-dimensional central deflections of an axially moving nano plate with $\hat{A}$ = 5% and (*Be*, *G*) = (0.2, 0.2) are plotted in Fig. 8 for uniform (Fig. 8(a)) and symmetric (Fig. 8(b)) GPL distributions, respectively. It is obvious in Fig. 8 that the dimensionless dynamic displacement of the plate increases with a rise in temperature values for both GPL distributions. In comparison with the symmetric GPL distribution (Fig. 8(b)), the influence of the temperature rise is far greater when the plate is reinforced with GPLs in pattern (Fig. 8(a)), see Fig 8(a).

Figs. 9(a) and (b), respectively, depict non-dimensional maximum dynamic deflection at the center versus temperature changes for various GPL weight fractions for CCCC and SSSS boundary conditions, respectively. It is presumed that *Be* = 0, *G* = 0.2 and GPL distribution is symmetric (Fig. 9(a)). From these figures, it is seen that the dynamic deflection variation due to a rise in the magnitude of temperature increases linearly when $\hat{A}$ = 0. However, by adding GPLs into the moving nanoplate, the vertical displacement increases nonlinearly with an increment in the amount of temperature. Such an increase is much more remarkable for $\hat{A}$ = 2%.

Fig. 10 depicts the variation in the central deflection for various velocities (Ω) for two types of edge constrains with GPL pattern: B, $\hat{A}$ = 5%. The results show that for both sets of boundary conditions the central deflection growths moderately until the critical velocity is taken placed, after that it tends to infinity. The obtained outcomes also demonstrate that boundary conditions have great influences on the critical velocity in which the nanoplate has the maximum displacements with respect to time variation. It is observed that the critical velocity of nanoplate with SSSS boundary condition is much greater than those with CCCC one.

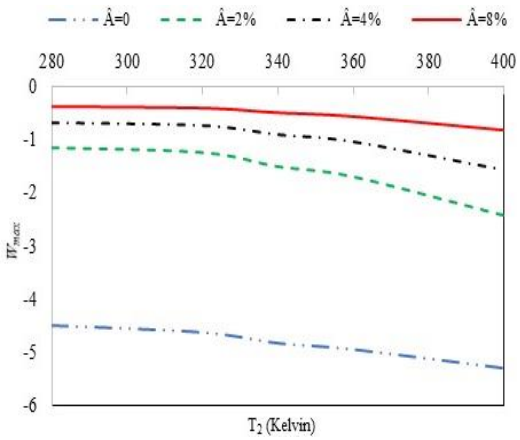

(a) CCCC

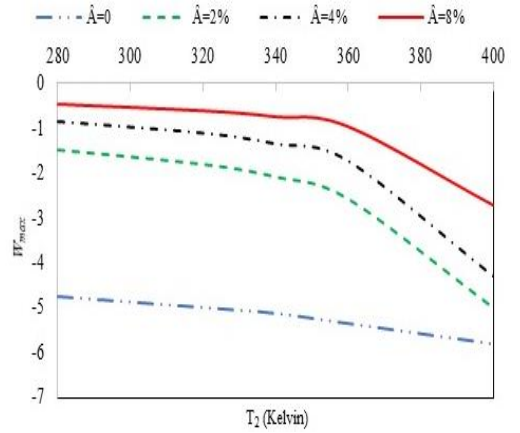

(b) SSSS

Fig. 9 Effects of temperature change and weight fraction of GPLs on the non-dimensional central displacement of the micro-size plate

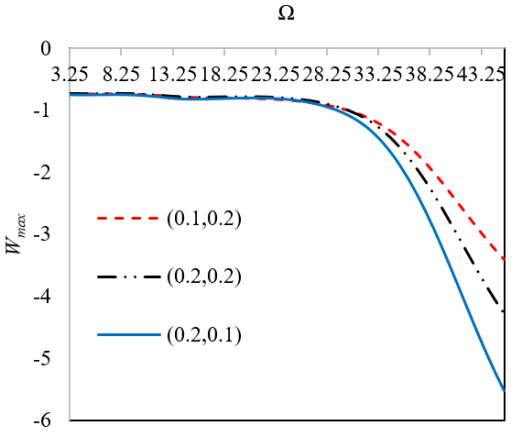

(a) CCCC

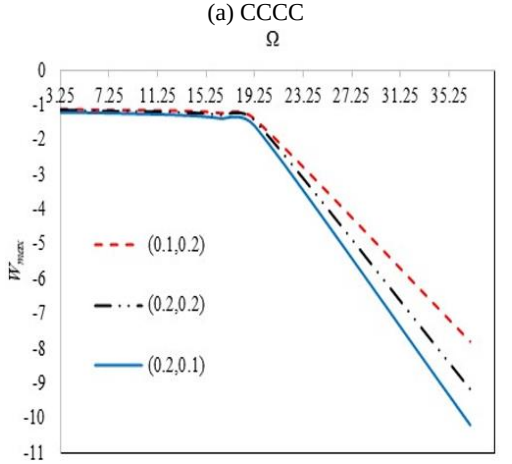

(b) SSSS

Fig. 10 Effects of velocity and nano-scale parameters (*Be*, *G*) on the dynamic displacement of the micro-size plate

6. Conclusions

In this paper, the time-dependent behaviors of GPL/ polymer nanoplates subjected to thermal and mechanical loads resting on elastic foundations with four-edge simply supported and clamped boundary conditions has been studied. The equations of motion have been developed based on FSDT along with the nonlocal strain gradient theory, and solved by the kinetic dynamic relaxation method coupled with the implicit Newmark method. In the current investigation, two types of GPL distributions have been considered, and the effects of graphene nano-particle distributions and weight coefficients, parameters of elastic foundation, temperature change, edge surroundings and the magnitudes of the plate speed have been analyzed. The following results are remarkable.

• Reinforcing the nanoplate with Graphene sheets can offer incredible and outstanding mechanical characteristics.

• Compared to uniform distribution, GPLs with symmetric one have the lower bending deformation.

• Compared to symmetric GPL distribution, the impact of the temperature increment on dynamic deflection is much greater once the plate is strengthened with GPLs in uniform pattern.

• Regarding temperature variations, an increase in discrepancy between T_2 and T_1 leads to higher dynamic deflection.

• The unstiffening effect of nonlocality and toughening influence of strain gradient parameter on dynamic behaviors of the nanoplate become more evident in higher values of the plate's velocity.

• The effects of the GPL distributions on the value of the critical velocity are small. However, boundary conditions have great impacts on the critical velocities.

• The effect of the Pasternak elastic foundation model on the reduction of dynamic deflection is more remarkable than that of its Winkler counterpart.

Good accuracy, low computational cost and the stability are the main features of the present computational techniques.

References

Abualnour, M., Chikh, A., Hebali, H., Kaci, A., Tounsi, A., Bousahla, A.A. and Tounsi, A. (2019), "Thermomechanical analysis of antisymmetric laminated reinforced composite plates using a new four variable trigonometric refined plate theory", *Comput. Concrete, Int. J.*, **24**(6), 489-498. https://doi.org/10.12989/cac.2019.24.6.489.

Akbaş, S.D. (2019), "Hygro-thermal nonlinear analysis of a

functionally graded beam", *J. Appl. Comput. Mech.*, **5**(2), 477-485. https://doi.org/10.22055/JACM.2018.26819.1360.

Al-Furjan, M., Habibi, M., Chen, G., Safarpour, H., Safarpour, M. and Tounsi, A. (2020a), "Chaotic oscillation of a multi-scale hybrid nano-composites reinforced disk under harmonic excitation via GDQM", *Compos. Struct.*, **252**, 112737. https://doi.org/10.1016/j.compstruct.2020.112737.

Al-Furjan, M.S.H., Habibi, M., Jung, D.W., Sadeghi, S., Safarpour, H., Tounsi, A. and Chen, G. (2020b), "A computational framework for propagated waves in a sandwich doubly curved nanocomposite panel", *Eng. Comput.*, **2020**, 1-18. https://doi.org/10.1007/s00366-020-01130-8.

Al-Furjan, M.S.H., Habibi, M., Rahimi, A., Chen, G., Safarpour, H., Safarpour, M. and Tounsi, A. (2020c), "Chaotic simulation of the multi-phase reinforced thermo-elastic disk using GDQM", *Eng. Comput.*, **229**(1), 94. https://doi.org/10.1007/s00366-020-01144-2.

Al-Furjan, M.S.H., Safarpour, H., Habibi, M., Safarpour, M. and Tounsi, A. (2020d), "A comprehensive computational approach for nonlinear thermal instability of the electrically FG-GPLRC disk based on GDQ method", *Eng. Comput.*, **2020**, 1-18. https://doi.org/10.1007/s00366-020-01088-7.

Al-Mashat, L., Shin, K., Kalantar-zadeh, K., Plessis, J.D., Han, S.H., Kojima, R.W., Kaner, R.B., Li, D., Gou, X., Ippolito, S.J. and Wlodarski, W. (2010), "Graphene/polyaniline nanocomposite for hydrogen sensing", *J. Phys. Chem. C*, **114**(39), 16168-16173. https://doi.org/10.1021/jp103134u.

Alamatian, J. (2012), "A new formulation for fictitious mass of the Dynamic Relaxation method with kinetic damping", *Comput. Struct.*, **90-91**, 42-54. https://doi.org/10.1016/j.compstruc.2011.10.010.

Alic, V. and Persson, K. (2016), "Form finding with dynamic relaxation and isogeometric membrane elements", *Comput. Methods Appl. Mech. Eng.*, **300**, 734-747. https://doi.org/10.1016/j.cma.2015.12.009.

An, C. and Su, J. (2011), "Dynamic response of clamped axially moving beams. Integral transform solution", *Appl. Math. Comput.*, **218**(2), 249-259. https://doi.org/10.1016/j.amc.2011.05.035.

Arani, A.G., Haghparast, E. and BabaAkbar Zarei, H. (2016), "Nonlocal vibration of axially moving graphene sheet resting on orthotropic visco-Pasternak foundation under longitudinal magnetic field", *Physica B Condens. Matter*, **495**, 35-49. https://doi.org/10.1016/j.physb.2016.04.039.

Asghar, S., Naeem, M.N., Hussain, M., Taj, M. and Tounsi, A. (2020), "Prediction and assessment of nonlocal natural frequencies of DWCNTs: Vibration analysis", *Comput. Concrete, Int. J.*, **25**(2), 133-144. https://doi.org/10.12989/cac.2020.25.2.133.

Balubaid, M., Tounsi, A., Dakhel, B. and Mahmoud, S.R. (2019), "Free vibration investigation of FG nanoscale plate using nonlocal two variables integral refined plate theory", *Comput. Concrete, Int. J.*, **24**(6), 579-586.

Barati, M.R. (2018), "A general nonlocal stress-strain gradient theory for forced vibration analysis of heterogeneous porous nanoplates", *Eur. J. Mech. A Solids*, **67**, 215-230. https://doi.org/10.1016/j.euromechsol.2017.09.001.

Bellal, M., Hebali, H., Heireche, H., Bousahla, A.A., Tounsi, A., Bourada, F. and Tounsi, A. (2020), "Buckling behavior of a single-layered graphene sheet resting on viscoelastic medium via nonlocal four-unknown integral model", *Steel Compos. Struct., Int. J.*, **34**(5), 643-655. https://doi.org/10.12989/scs.2020.34.5.643.

Bendenia, N., Zidour, M., Bousahla, A.A., Bourada, F., Tounsi, A., Benrahou, K.H. and Tounsi, A. (2020), "Deflections, stresses and free vibration studies of FG-CNT reinforced sandwich plates resting on Pasternak elastic foundation", *Comput. Concrete, Int. J.*, **26**(3), 213-226. https://doi.org/10.12989/cac.2020.26.3.213.

Berghouti, H., Adda Bedia, E.A., Benkhedda, A. and Tounsi, A. (2019), "Vibration analysis of nonlocal porous nanobeams made of functionally graded material", *Adv. Nano Res., Int. J.*, **7**(5), 351-364. https://doi.org/10.12989/anr.2019.7.5.351.

Bourada, F., Bousahla, A.A., Tounsi, A., Bedia, E.A.A., Mahmoud, S.R., Benrahou, K.H. and Tounsi, A. (2020), "Stability and dynamic analyses of SW-CNT reinforced concrete beam resting on elastic-foundation", *Comput. Concrete, Int. J.*, **25**(6), 485-495. https://doi.org/10.12989/cac.2020.25.6.485.

Bousahla, A.A., Bourada, F., Mahmoud, S.R., Tounsi, A., Algarni, A., Bedia, E.A.A. and Tounsi, A. (2020), "Buckling and dynamic behavior of the simply supported CNT-RC beams using an integral-first shear deformatin theory", *Comput. Concrete, Int. J.*, **25**(2), 155-166. https://doi.org/10.12989/cac.2020.25.2.155.

Boussoula, A., Boucham, B., Bourada, M., Bourada, F., Tounsi, A., Bousahla, A.A. and Tounsi, A. (2020), "A simple nth-order shear deformation theory for thermomechanical bending analysis of different configurations of FG sandwich plates", *Smart Struct. Syst., Int. J.*, **25**(2), 197-218. https://doi.org/10.12989/sss.2020.25.2.197.

Boutaleb, S., Benrahou, K.H., Bakora, A., Algarni, A., Bousahla, A.A., Tounsi, A. and Mahmoud, S.R. (2019), "Dynamic analysis of nanosize FG rectangular plates based on simple nonlocal quasi 3D HSDT", *Adv. Nano Res., Int. J.*, **7**(3), 191-208. http://dx.doi.org/10.12989/anr.2019.7.3.191.

Chen, D., Yang, J. and Kitipornchai, S. (2017), "Nonlinear vibration and postbuckling of functionally graded graphene reinforced porous nanocomposite beams", *Compos. Sci. Technol.*, **142**, 235-245. https://doi.org/10.1016/j.compscitech.2017.02.008.

Chikr, S.C., Kaci, A., Bousahla, A.A., Bourada, F., Tounsi, A., Bedia, E.A.A. and Tounsi, A. (2020), "A novel four-unknown integral model for buckling response of FG sandwich plates resting on elastic foundations under various boundary conditions using Galerkin's approach", *Geomech. Eng., Int. J.*, **21**(5), 471-487. https://doi.org/10.12989/gae.2020.21.5.471.

Cong, P.H. and Duc, N.D. (2018), "New approach to investigate the nonlinear dynamic response and vibration of a functionally graded multilayer graphene nanocomposite plate on a viscoelastic Pasternak medium in a thermal environment", *Acta Mech.*, **229**(9), 3651-3670. https://doi.org/10.1007/s00707-018-2178-3.

Draoui, A., Zidour, M., Tounsi, A. and Adim, B. (2019), "Static and dynamic behavior of nanotubes-reinforced sandwich plates using FSDT", *J. Nano Res.*, **57**, 117-135. https://doi.org/10.4028/www.scientific.net/JNanoR.57.117.

Ebrahimi, F. and Dabbagh, A. (2019), "Vibration analysis of multi-scale hybrid nanocomposite plates based on a Halpin-Tsai homogenization model", *Compos. Part B Eng.*, **173**, 106955. https://doi.org/10.1016/j.compositesb.2019.106955.

Ebrahimi, F., Karimiasl, M. and Selvamani, R. (2020), "Bending analysis of magneto-electro piezoelectric nanobeams system under hygro-thermal loading", *Adv. Nano Res.*, **8**(3), 203-214. https://doi.org/10.12989/anr.2020.8.3.203.

Esmaeilzadeh, M. and Kadkhodayan, M. (2018), "Nonlinear dynamic analysis of an axially moving porous FG plate subjected to a local force with kinetic dynamic relaxation method", *Comput. Methods Mater. Sci.*, **18**(1), 18-28.

Esmaeilzadeh, M. and Kadkhodayan, M. (2019a), "Dynamic analysis of stiffened bi-directional functionally graded plates with porosities under a moving load by dynamic relaxation method with kinetic damping", *Aerosp. Sci. Technol.*, **93**, 105333. https://doi.org/10.1016/j.ast.2019.105333.

Esmaeilzadeh, M. and Kadkhodayan, M. (2019b), "Numerical

investigation into dynamic behaviors of axially moving functionally graded porous sandwich nanoplates reinforced with graphene platelets", *Mater. Res. Express*, **6**(10), 1050b7. https://doi.org/10.1088/2053-1591/ab407b.

Gafour, Y., Hamidi, A., Benahmed, A., Zidour, M. and Bensattalah, T. (2020), "Porosity-dependent free vibration analysis of FG nanobeam using non-local shear deformation and energy principle", *Adv. Nano Res., Int. J.*, **8**(1), 37-47. https://doi.org/10.12989/anr.2020.8.1.037.

Golmakani, M.E. and Zeighami, V. (2017), "Nonlinear thermo-elastic bending of functionally graded carbon nanotube-reinforced composite plates resting on elastic foundations by dynamic relaxation method", *Mech. Adv. Mater. Struct.*, **25**(10), 868-880. https://doi.org/10.1080/15376494.2017.1310336.

Hanifehlou, S. and Mohammadimehr, M. (2020), "Buckling analysis of sandwich beam reinforced by GPLs using various shear deformation theories", *Comput. Concrete, Int. J.*, **25**(5), 427-432. https://doi.org/10.12989/cac.2020.25.5.427.

Hussain, M., Naeem, M.N., Tounsi, A. and Taj, M. (2019), "Nonlocal effect on the vibration of armchair and zigzag SWCNTs with bending rigidity", *Adv. Nano Res., Int. J.*, **7**(6), 431-442. https://doi.org/10.12989/anr.2019.7.6.431.

Kaddari, M., Kaci, A., Bousahla, A.A., Tounsi, A., Bourada, F., Tounsi, A. and Al-Osta, M.A. (2020), "A study on the structural behaviour of functionally graded porous plates on elastic foundation using a new quasi-3D model: Bending and free vibration analysis", *Comput. Concrete, Int. J.*, **25**(1), 37-57. https://doi.org/10.12989/cac.2020.25.1.037.

Li, C., Liu, J.J., Cheng, M. and Fan, X.L. (2017), "Nonlocal vibrations and stabilities in parametric resonance of axially moving viscoelastic piezoelectric nanoplate subjected to thermo-electro-mechanical forces", *Compos. Part B Eng.*, **116**, 153-169. https://doi.org/10.1016/j.compositesb.2017.01.071.

Li, Q., Di, W., Chen, X., Liu, L., Yu, Y. and Gao, W. (2018), "Nonlinear vibration and dynamic buckling analyses of sandwich functionally graded porous plate with graphene platelet reinforcement resting on Winkler-Pasternak elastic foundation", *Int. J. Mech. Sci.*, **148**, 596-610. https://doi.org/10.1016/j.ijmecsci.2018.09.020.

Liebold, C. and Müller, W. (2015), "Applications of strain gradient theories to the size effect in submicro-structures incl. experimental analysis of elastic material parameters", *Bull. TICMI*, **19**(1), 45-55.

Lim, C.W., Zhang, G. and Reddy, J.N. (2015), "A higher-order nonlocal elasticity and strain gradient theory and its applications in wave propagation", *J. Mech. Phys. Solids*, **78**, 298-313. https://doi.org/10.1016/j.jmps.2015.02.001.

Liu, H., Lv, Z. and Wu, H. (2019), "Nonlinear free vibration of geometrically imperfect functionally graded sandwich nanobeams based on nonlocal strain gradient theory", *Compos. Struct.*, **214**, 47-61. https://doi.org/10.1016/j.compstruct.2019.01.090.

Mahmoudi, A., Benyoucef, S., Tounsi, A., Benachour, A., Adda Bedia, E.A. and Mahmoud, S. (2019), "A refined quasi-3D shear deformation theory for thermo-mechanical behavior of functionally graded sandwich plates on elastic foundations", *J. Sandw. Struct. Mater.*, **21**(6), 1906-1929. https://doi.org/10.1177/1099636217727577.

Matouk, H., Bousahla, A.A., Heireche, H., Bourada, F., Bedia, E.A.A., Tounsi, A. and Benrahou, K.H. (2020), "Investigation on hygro-thermal vibration of P-FG and symmetric S-FG nanobeam using integral Timoshenko beam theory", *Adv. Nano Res., Int. J.*, **8**(4), 293-305. https://doi.org/10.12989/anr.2020.8.4.293.

Medani, M., Benahmed, A., Zidour, M., Heireche, H., Tounsi, A., Bousahla, A.A. and Mahmoud, S.R. (2019), "Static and dynamic behavior of (FG-CNT) reinforced porous sandwich plate using energy principle" *Steel Compos. Struct., Int. J.*, **32**(5), 595-610. https://doi.org/10.12989/scs.2019.32.5.595.

Mohammadimehr, M. and Meskini, M. (2020), "Analysis of porous micro sandwich plate: Free and forced vibration under magneto-electro-elastic loadings", *Adv. Nano Res., Int. J.*, **8**(1), 69-82. https://doi.org/10.12989/anr.2020.8.1.069.

Pashmforoush, F. (2020), "Finite element analysis of low velocity impact on carbon fibers/carbon nanotubes reinforced polymer composites", *J. Appl. Comput. Mech.*, **6**(3), 383-393. https://doi.org/10.22055/JACM.2019.29072.1554.

Rabhi, M., Benrahou, K.H., Kaci, A., Houari, M.S.A., Bourada, F., Bousahla, A.A. and Tounsi, A. (2020), "A new innovative 3-unknowns HSDT for buckling and free vibration of exponentially graded sandwich plates resting on elastic foundations under various boundary conditions", *Geomech. Eng., Int. J.*, **22**(2), 119-132. https://doi.org/10.12989/gae.2020.22.2.119.

Rafiee, M.A., Rafiee, J., Wang, Z., Song, H., Yu, Z.Z. and Koratkar, N. (2009), "Enhanced mechanical properties of nanocomposites at low graphene content", *ACS Nano*, **3**(12), 3884-3890. https://doi.org/10.1021/nn9010472.

Reddy, M.R., Karunasena, W. and Lokuge, W. (2018), "Free vibration of functionally graded-GPL reinforced composite plates with different boundary conditions", *Aerosp. Sci. Technol.*, **78**, 147-156. https://doi.org/10.1016/j.ast.2018.04.019.

Refrafi, S., Bousahla, A.A., Bouhadra, A., Menasria, A., Bourada, F., Tounsi, A. and Tounsi, A. (2020), "Effects of hygro-thermo-mechanical conditions on the buckling of FG sandwich plates resting on elastic foundations", *Comput. Concrete, Int. J.*, **25**(4), 311-325. https://doi.org/10.12989/cac.2020.25.4.311.

Shen, H.S., Lin, F. and Xiang, Y. (2017), "Nonlinear bending and thermal postbuckling of functionally graded graphene-reinforced composite laminated beams resting on elastic foundations", *Eng. Struct.*, **140**, 89-97. https://doi.org/10.1016/j.engstruct.2017.02.069.

Shishesaz, M., Shariati, M. and Yaghootian, A. (2020), "Nonlocal elasticity effect on linear vibration of nano-circular plate using adomian decomposition method", *J. Appl. Comput. Mech.*, **6**(1), 63-76. https://doi.org/10.22055/JACM.2019.28504.1488.

Song, M., Kitipornchai, S. and Yang, J. (2017), "Free and forced vibrations of functionally graded polymer composite plates reinforced with graphene nanoplatelets", *Compos. Struct.*, **159**, 579-588. https://doi.org/10.1016/j.compstruct.2016.09.070.

Song, M., Gong, Y., Yang, J., Zhu, W. and Kitipornchai, S. (2019), "Free vibration and buckling analyses of edge-cracked functionally graded multilayer graphene nanoplatelet-reinforced composite beams resting on an elastic foundation", *J. Sound Vib.*, **458**, 89-108. https://doi.org/10.1016/j.jsv.2019.06.023.

Tayeb, T.S., Zidour, M., Bensattalah, T., Heireche, H., Benahmed, A. and Bedia, E.A.A. (2020), "Mechanical buckling of FG-CNTs reinforced composite plate with parabolic distribution using Hamilton's energy principle", *Adv. Nano Res., Int. J.*, **8**(2), 135-148. https://doi.org/10.12989/anr.2020.8.2.135.

Tounsi, A., Al-Dulaijan, S.U., Al-Osta, M.A., Chikh, A., Al-Zahrani, M.M., Sharif, A. and Tounsi, A. (2020), "A four variable trigonometric integral plate theory for hygro-thermo-mechanical bending analysis of AFG ceramic-metal plates resting on a two-parameter elastic foundation", *Steel Compos. Struct., Int. J.*, **34**(4), 511-524. https://doi.org/10.12989/scs.2020.34.4.511.

Wang, Y., Feng, C., Santiuste, C., Zhao, Z. and Yang, J. (2019a), "Buckling and postbuckling of dielectric composite beam reinforced with graphene platelets (GPLs)", *Aerosp. Sci. Technol.*, **91**, 208-218. https://doi.org/10.1016/j.ast.2019.05.008.

Wang, Y., Xie, K., Shi, C. and Fu, T. (2019b), "Nonlinear bending of axially functionally graded microbeams reinforced by

graphene nanoplatelets in thermal environments", *Mater*. *Res*. *Express*, **6**(8), 85615. https://doi.org/10.1088/2053-1591/ab1eef.

Wu, H., Yang, J. and Kitipornchai, S. (2017), "Dynamic instability of functionally graded multilayer graphene nanocomposite beams in thermal environment", *Compos*. *Struct*., **162**, 244-254. https://doi.org/10.1016/j.compstruct.2016.12.001.

Yang, B., Yang, J. and Kitipornchai S. (2017), "Thermoelastic analysis of functionally graded graphene reinforced rectangular plates based on 3D elasticity", *Meccanica*, **52**(10), 2275-2292. https://doi.org/10.1007/s11012-016-0579-8.

Yang, J., Chen, D. and Kitipornchai, S. (2018), "Buckling and free vibration analyses of functionally graded graphene reinforced porous nanocomposite plates based on Chebyshev-Ritz method", *Compos*. *Struct*., **193**, 281-294. https://doi.org/10.1016/j.compstruct.2018.03.090.

Zhang, Y.W., Zhang, Z., Chen, L.Q., Yang, T.Z., Fang, B. and Zang, J. (2015), "Impulse-induced vibration suppression of an axially moving beam with parallel nonlinear energy sinks", *Nonlin*. *Dyn*., **82**(1-2), 61-71. https://doi.org/10.1007/s11071-015-2138-6.

Zhang, Y.F., Zhao, Y.H., Bai, S.L. and Yuan, X. (2016), "Numerical simulation of thermal conductivity of graphene filled polymer composites", *Compos*. *Part B Eng*., **106**, 324-331. https://doi.org/10.1016/j.compositesb.2016.09.052.

Zhu, R., Pan, E. and Roy, A.K. (2007), "Molecular dynamics study of the stress-strain behavior of carbon-nanotube reinforced Epon 862 composites", *Mater*. *Sci*. *Eng*. *A*, **447**(1-2), 51-57. https://doi.org/10.1016/j.msea.2006.10.054.

AT